Korean J. Chem. Eng., 37(8), 1440-1444 (2020)
DOI: 10.1007/s11814-020-0623-1

pISSN: 0256-1115
eISSN: 1975-7220

Surface decorated $La_{0.43}Ca_{0.37}Ni_{0.06}Ti_{0.94}O_{3-d}$ as an anode functional layer for solid oxide fuel cell applications

HyeonGwon Jeong*, Doyeub Kim, Bharat Sharma*, Jong Hyeok Noh*, Kang Taek Lee***,†, and Jae-ha Myung*,†**

*Department of Materials Science and Engineering, Incheon National University, Incheon 22012, Korea
**Department of Energy Science and Engineering, Daegu Gyeongbuk Institute of Science and Technology (DGIST), Daegu 42988, Korea
***Department of Mechanical Engineering, Korea Advanced Institute of Science and Technology (KAIST), Daejeon 34141, Korea

(*Received 20 April 2020 • Revised 29 May 2020 • Accepted 30 June*)

Abstract−Surface decorated $La_{0.43}Ca_{0.37}Ni_{0.06}Ti_{0.94}O_{3-d}$ (LCNT) perovskite oxide was investigated as an anode functional layer (AFL) for anode-supported solid oxide fuel cells (SOFCs). The surface exsolved Ni nano particles on LCNT scaffold enlarged electrochemically active triple phase boundaries (TPBs) without any agglomeration and mechanical failure. The Ni particles with 60 nm in diameter were homogeneously exsolved from LCNT perovskite. The Ni-YSZ anode supported cell with LCNT anode functional layer (AFL) exhibited a maximum power density of 0.94 W/cm^2, similar to that of the conventional Ni-YSZ AFL cell at 900 °C. The activation polarization resistance of the LCNT AFL cell was effectively reduced compared to that of the Ni-YSZ AFL cell, though it had higher Ohmic resistance due to thicker YSZ electrolyte and lower electrical conductivity. Our study suggests the potential use of LCNT with exsolved nano particles as an active and durable AFL for high-temperature SOFCs.

Keywords: SOFC, Exsolution, Anode Functional Layer, Metal Nano Particles, Perovskite

INTRODUCTION

The utilization of hydrogen energy is one of the most needed technologies to meet soaring energy demand in clear and sustainable manner. Solid oxide fuel cells (SOFCs) attract attention for their high conversion efficiency with great fuel flexibility. The performance and durability of SOFCs are largely determined by their electrode material properties. The anode material for SOFCs must be physically and chemically stable under severe operating conditions while conducting both electrons and ions with appropriate catalytic activity. In this regard, a porous cermet material of Ni and YSZ (stabilized zirconia) mixture has been widely used as anode for SOFCs [1-3]. Recent studies in the advancement of anode electrode are mainly under the approach to increase electrochemically active surface area by tailoring its microstructure [4]. Fabrication of anode functional layer (AFL) adjacent to thin electrolyte is one of the feasible solutions for commercially available anode-supported SOFC devices [5-7]. The design of AFL is commonly focused on enlarging triple phase boundaries (TPBs) by reducing porosity and difference of thermal expansion coefficient (TEC) value with slightly increased YSZ ratio, while the supporting layer has high nickel concentration and pore distribution to ensure sufficient electronic conductivity and gas transfer rate [5,8]. These kinds of multi-layered anode structures could improve electrochemical performances; however, increased YSZ concentration in the functional layer constrains the catalytically active surface area [9-12].

Recently developed in-situ exsolution method has been suggested as a new concept for innovative SOFCs electrode design. Metal catalysts are dissolved inside the perovskite lattice structure in oxidizing conditions and exsolved on the surface as highly dispersed nanoparticles under reducing atmosphere [4,13-15]. The exsolution based electrode materials are mixed ionic and electronic conductors (MIECs) as well as high catalytic activity, which could play a key role in overcoming the limited TPBs problem arising from simple YSZ ionic conductor. Neagu et al. revealed extraordinary chemical and thermal stability of nickel nano exsolved particles on the A-site deficient perovskite mother phase compared with vapor-deposited nickel particles [14]. Previously, our group reported an innovative approach to maximize the surface exsolution of nickel nanoparticles on perovskite-based electrode within a few seconds by applying electrical polarization under operating condition [17]. The studies further demonstrated that perovskite-based oxides, which were highly desirable properties for exsolution materials, could improve performance and stability of the all-ceramic SOFCs [18,19].

In this study, the surface exsolved anode functional layer (AFL) with Ni nanoparticles was introduced to increase TPBs and structural stability for anode-supported SOFCs. The conventional Ni-YSZ cermet AFL was substituted with A-site deficient $La_{0.43}Ca_{0.37}Ni_{0.06}Ti_{0.94}O_{3-d}$ (LCNT) as an MIEC high catalytic activity. The morphological properties and electrochemical performance of anode-supported SOFCs using LCNT AFL were investigated and evaluated for efficient fuel cell reaction at various operating temperatures.

†To whom correspondence should be addressed.
E-mail: mjaeha@inu.ac.kr, leekt@kaist.ac.kr

EXPERIMENTAL

1. Materials Synthesis

The $La_{0.43}Ca_{0.37}Ni_{0.06}Ti_{0.94}O_{3-d}$ (LCNT) perovskite powder was prepared by the solid-state reaction method. Under stoichiometric consideration, starting materials La_2O_3 (Alfa Aesar, Lanthanum(III) oxide, reaction 99.9% (REO) powder), TiO_2 (Sigma Aldrich, Titanium(IV) oxide anatase powder 99.8% trace metal base), $CaCO_3$ (Alfa Aesar, Calcium carbonate, 99.5% (metal basis)) and $Ni(NO_3)_2 \cdot 6H_2O$ (Acros Organics, Nickel(II) nitrate hexahydrate, 99%, for analysis) were mixed with deionized water and stirred for 24 h. The dehydrated precursor mixture was isostatically pressed as a pellet and then sintered at 1,000 °C for 3 h to stimulate phase nucleation. The gray-colored pellet was ground and sintered again at 1,400 °C for 3 h to obtain single-phase perovskite substrate materials. The sintered LCNT pellets were finally ground by planetary milling at 500 rpm for 4 h to optimize the size distribution for AFL fabrication.

2. Cell Fabrication

The electrolyte and anode functional layer (AFL) were prepared by conventional dip-coating and screen-printing method, respectively. NiO (Kojundo chemical laboratory, Co., Ltd) and YSZ (TZ8Y, Tosho) powder were physically mixed at a weight ratio of 60 : 40 with 20 wt% of additional carbon black (CB). The average particle size of NiO and YSZ powder was 0.71 and 0.04 μm, respectively. The homogeneously mixed powder was then die-pressed and sintered at 1,100 °C for 3 h to obtain porous anode substrate. The AFL inks (NiO-YSZ, LCNT) were prepared by high energy milling, then screen printed on the pellet and sintered at 1,200 °C for 3 h to obtain stable and porous bi-layered anode structure without delamination. The YSZ electrolyte layer was fabricated by step dip-coating method to avoid possible defect formation between AFL and thin electrolyte interface. The first dip-coated pellets were pre-sintered at 1,200 °C for 3 h and then the stabilized porous electrolyte layer was dip-coated again before the second sintering process to get dense electrolyte. The high temperature sintered anode support was mechanically ground to reach the optimal thickness (800 μm). The LSM-YSZ cathode (weight ratio of 50 : 50) electrode was finally screen printed on the dense electrolyte layer (20 μm of thickness) and sintered at 1,100 °C for 3 h to get the appropriate microstructure for its oxygen kinetic reactions. The detailed microstructure of unit cells is illustrated on Fig. 1.

3. Material Characterization and Electrochemical Properties

A structural analysis of synthesized $La_{0.43}Ca_{0.37}Ni_{0.06}Ti_{0.94}O_{3-d}$ (LCNT) was performed by XRD (Smart Lab., Rigaku) in a range of 20°-80° with Rietveld refinement method. The configuration of the electrode and electrolyte layers was analyzed by using FE-SEM (JSM-7001F, JEOL). The average pore distribution of the Ni-YSZ supporting layer and different types of AFL was characterized by a cross-sectional SEM image. The chemical stability of AFL materials should be considered because of the high-temperature process of SOFCs fabrication. In this regard, physically mixed NiO and LCNT pellets were prepared and sintered at the highest process temperature (~1,350 °C) to confirm reactivity between inter-layers.

To evaluate electrochemical properties of single cells with various AFLs, prepared samples were mounted on alumina tube and reduced at 900 °C for 1 h under wet hydrogen atmosphere (3% H_2/H_2O). The current-voltage curve was collected by linear sweep voltammetry (LSV) at scanning rate of 50 mv/s with 200 sccm of wet hydrogen fuel and 500 sccm of dry air. Electrochemical impedance spectroscopy (EIS) and equivalent circuit model of $L_1R_\Omega(C_1/R_1)(C_2/R_2)(C_3/R_3)$ were introduced to identify rate-limiting factor of each sample at an open-circuit voltage (OCV) from 700 to 900 °C.

RESULTS AND DISCUSSION

1. Materials Characterization

Fig. 2(a) and (b) show the XRD analysis of LCT and LCNT with Rietveld refinement result. Both LCT and LCNT materials were synthesized as a tetragonal perovskite structure with the space group of Ibnm. The slightly increased lattice constant of LCNT (3.866 Å) compared with LCT (3.862 Å) implies successful doping of bigger Ni^{2+} ions inside the smaller Ti^{+4} host sites. As Fig. 2(c) indicates, the physical mixture of NiO and LCNT revealed stable even after high temperature (~1,350 °C) sintering process, suggesting that LCNT could be one of the appropriate materials for functional layer without any unwanted chemical reaction between NiO and YSZ based microstructure.

2. Morphological Analysis

Fig. 3(a) shows the cross-sectional surface SEM image of single cell without AFL. As shown in Fig. 3(b) and (c), the thickness of

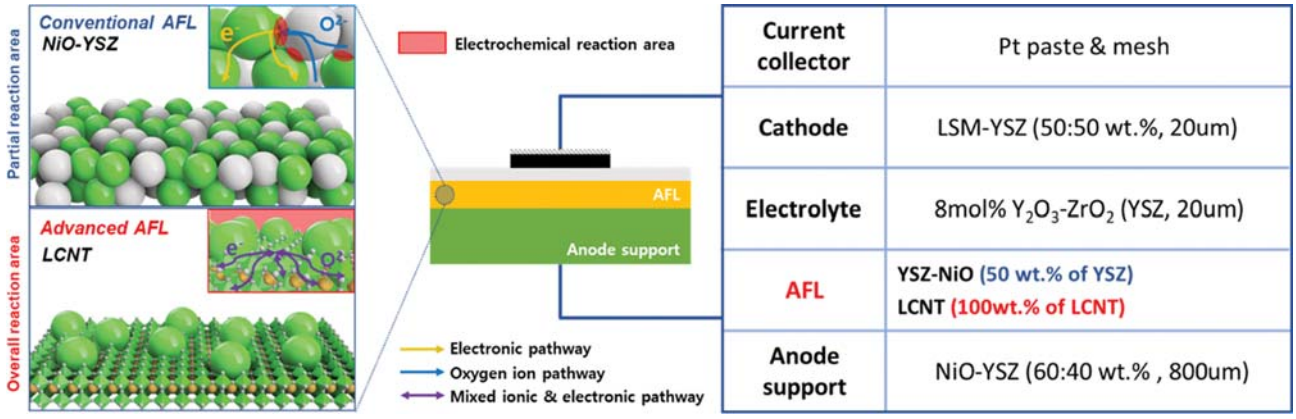

Fig. 1. Schematic illustration of anode-supported unit cells with different anode functional layers (AFLs).

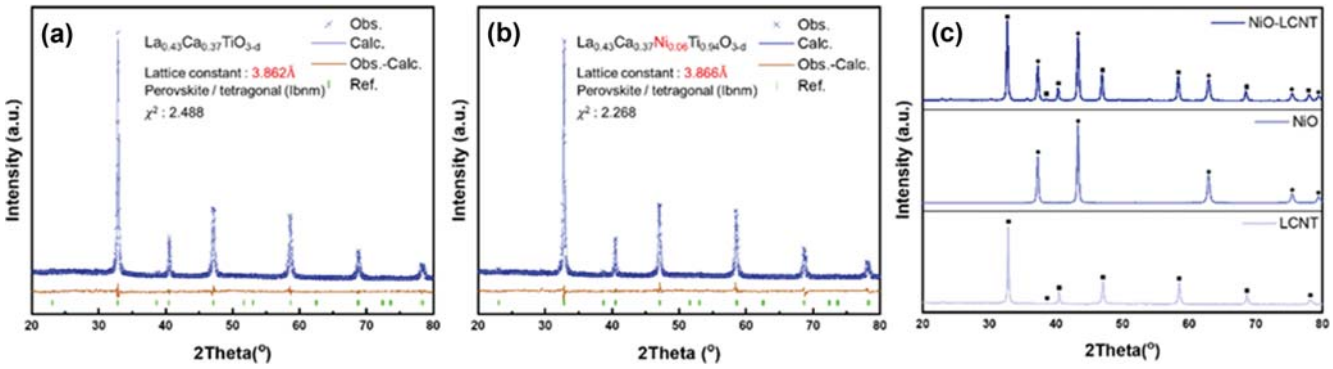

Fig. 2. XRD results after Rietveld refinement of (a) $La_{0.43}Ca_{0.37}TiO_{3-d}$, (b) $La_{0.43}Ca_{0.37}Ni_{0.06}Ti_{0.94}O_{3-d}$, (c) NiO-LCNT mixture. The structural parameter used in refinement is a=5.47, b=5.47, c=7.73, α=90.0 β=90.0 γ=90.0.

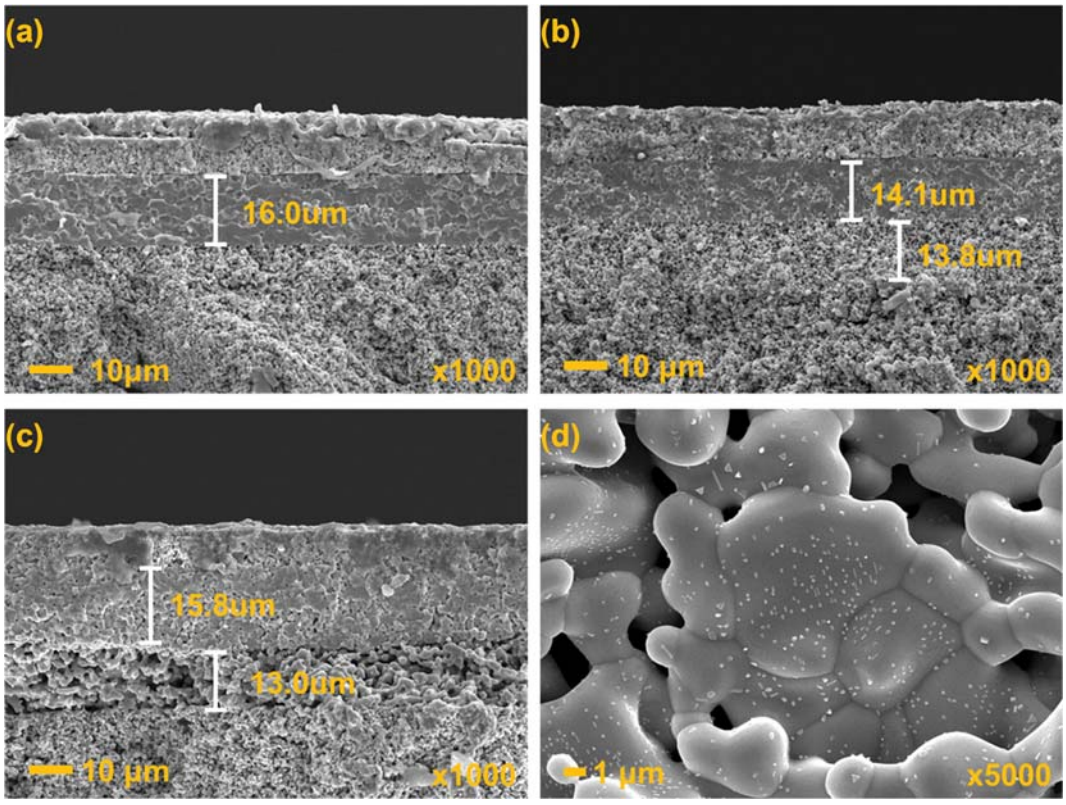

Fig. 3. SEM images of (a) the reference cell without AFL, (b) with conventional NiO-YSZ AFL (c) LCNT AFL, (d) surface of LCNT AFL after exsolution.

AFL is controlled to 13.8 μm and 13.0 μm for conventional Ni-YSZ and LCNT to overcome the inherent low electronic conductivity of perovskite oxide. The pore concentration of AFL was calculated to 25% for Ni-YSZ and 20% for LCNT, improving both connectivity and active surface area in anode microstructure. The YSZ electrolyte layer was intended to thick enough to avoid possible permeation of gases between anode and cathode, in that the final co-sintering temperature (up to 1,350 °C) for dense electrolyte. Fig. 3(d) shows highly dispersed Ni nanoparticles on LCNT perovskite structure after the fuel cell test. The Ni nanoparticles embedded on the perovskite scaffold exhibited stable morphology without growth of particles and agglomeration at high temperature operating conditions. The particle sizes of exsolved Ni particles were around 30-60 nm in diameter. The overall morphological properties of

Table 1. Characteristics of three type unit cells

	Reference cell	Conventional AFL	LCNT AFL
Thickness of electrolyte	16.0 μm	14.1 μm	15.8 μm
Thickness of AFL	-	13.8 μm	13.0 μm
Porosity of AFL	-	25%	20%
Porosity of anode support		40%	

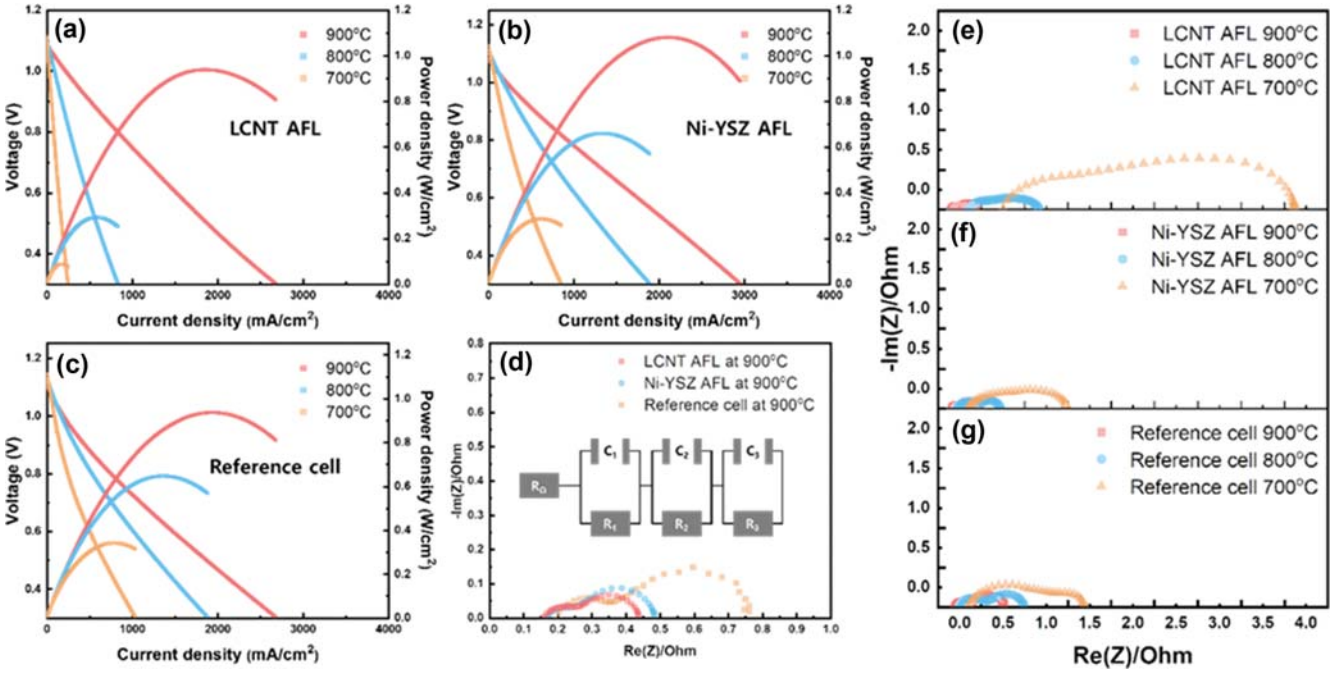

Fig. 4. I-V curves of (a) LCNT AFL, (b) Ni-YSZ AFL, (c) reference cell and impedance spectra for (d) three type unit cells at 900 °C and for (e)-(g) LCNT AFL, Ni-YSZ AFL, reference cells from 700 °C to 900 °C.

prepared samples are summarized in Table 1. The microstructure of LCNT AFL single cell had no observable crack and delamination between the electrode and electrolyte layer, indicating the structural stability of the perovskite-based oxide layer for the general architecture of SOFCs.

3. Electrochemical Properties

Fig. 4(a), (b) and (c) show I-V and power density curves of single cells with LCNT AFL, Ni-YSZ AFL, and without AFL (as a reference cell), respectively. The theoretically close OCV value of each sample indicates that the YSZ electrolyte layer is sufficiently sintered without any gas leakage. The peak power density of LCNT, Ni-YSZ, and reference cells recorded 0.94, 1.08 and 0.94 W/cm^2, where the Ni-YSZ and LCNT AFL sample presents minor power density difference. After decreasing operating temperature to 700 °C, the LCNT AFL sample showed the most drastic power density drop among the prepared button cells. This tendency is also supported by the Nyquist plot of Fig. 4(e), (f) and (g), indicating the increased polarization resistance of LCNT compared with others. As discussed later, the crucial drop in the power density of the LCNT AFL sample probably originated from diminished oxygen vacancy concentration and conducting properties of perovskite materials at lowered temperatures. The impedance spectra of each sample were fitted using an equivalent circuit model of $L_1R_\Omega(C_1/R_1)(C_2/R_2)(C_3/R_3)$, which has been widely adopted for anode supported SOFCs on various studies (Fig. 4(d)) [18,25,26]. In the proposed model, L_1 (inductance) corresponds to lead wire of testing environment, R_Ω is ohmic resistance between anode and cathode and three (C_n/R_n) components are non-ohmic losses of each electrochemical reaction steps, where the R_1, R_2, and R_3 are mainly defined as activation polarization, gas transfer and conversion reactions, respectively. The recorded impedance spectra include cathode impedance; however, we believe that the dominant polarization resistances could be attributed to anode support and functional layer because of employing the same cathode and electrolyte materials.

Table 2. Summarized impedance data using $L_1R_\Omega(C_1/R_1)(C_2/R_2)(C_3/R_3)$ model

	R_Ω (Ω·cm^2)	R_1 (Ω·cm^2)	R_2 (Ω·cm^2)	R_3 (Ω·cm^2)
Reference 900 °C	0.16	0.21	0.10	0.30
Reference 800 °C	0.21	0.37	0.047	0.37
Reference 700 °C	0.30	0.93	0.018	0.47
Ni-YSZ 900 °C	0.084	0.18	0.15	0.070
Ni-YSZ 800 °C	0.19	0.19	0.070	0.27
Ni-YSZ 700 °C	0.28	0.59	0.16	0.48
LCNT 900 °C	0.13	0.10	0.087	0.12
LCNT 800 °C	0.14	0.54	0.42	0.090
LCNT 700 °C	0.47	1.3	1.2	1.3

In Table 2, LCNT and Ni-YSZ samples showed lower ohmic resistance (R_Ω) than that of the reference cell at 900 °C, suggesting that the functional layers in prepared sample reduced contact resistance with electrolyte. The smaller R_Ω (0.130 Ω-cm^2) value of LCNT compared with reference cell (0.155 Ω-cm^2) and Ni-YSZ sample (0.084 Ω-cm^2) indicates that even perovskite material with low electronic conductivity could be considered as an alternative to conventional Ni-YSZ cermet material by optimizing its microstructure. The reduced activation resistance (R_1) of LCNT (0.104 Ω-cm^2) could compensate for the slightly higher ohmic resistance (0.130 Ω-cm^2), resulting in the lowest total impedance at 900 °C. The lowest activation losses of LCNT are due to the increased TPBs by nano-sized

Ni particles even with the lower amount of Ni loading compared with Ni-YSZ AFL. As operating temperature decreased to 800 °C, the total impedance of LCNT (1.183 Ω-cm^2) became higher than that of reference (0.998 Ω-cm^2) and Ni-YSZ sample (0.719 Ω-cm^2). The high-frequency range of R_1 value in LCNT was thermally activated from (0.104 Ω-cm^2) to (0.535 Ω-cm^2); on the other hand, Ni-YSZ and reference sample exhibited minor difference (0.01-0.11 Ω-cm^2) after reduced temperatures. This observation suggests that the YSZ scaffold in the functional layer was less susceptible to temperature. Such degradation of LCNT perovskite AFL is probably related to the reduced oxygen vacancy in LCNT perovskite scaffold at low operating temperature. At high operating temperature, the host Ti^{4+} ions in LCNT perovskite scaffold could be easily reduced to Ti^{3+} ions with formation of oxygen vacancy (V_o), therefore improving cell performance. As operating temperature decreased, however, the concentration of oxygen vacancy in LCNT was drastically decreased by relatively higher energy to reduce Ti^{4+} ions, which also decreased the cell performance of LCNT AFL cell [27-29]. Thus, we believe that LCNT AFL materials are more suitable for high-temperature devices, providing high catalytic activity and stability.

CONCLUSION

We designed Ni-doped single-phase perovskite-based oxide as a functional layer in an anode supported SOFC, suggesting that in-situ exsolved Ni nanoparticles can reduce activation polarization at high operating temperatures by increasing TPB sites. The microstructure of functional layer was stable without any delamination between adjacent YSZ electrolyte or supporting layer. The increased contact area and controlled thickness of LCNT AFL could reduce the ohmic resistance similar to that of conventional Ni-YSZ AFL materials. At high operating temperature (900 °C), the high electrocatalytic activity of LCNT AFL could compensate relatively low electrical conductivity in its total polarization resistances. The thermally and chemically stable nanostructure of LCNT AFL is regarded to enable the direct oxidation of various fuels such as hydrocarbon in SOFCs.

ACKNOWLEDGEMENTS

This work was supported by Incheon National University (International Cooperative) Research Grant in 2018 and by National Research Foundation of Korea (NRF-2018R1C1B5044487).

REFERENCES

1. P. I. Cowin, C. T. G. Petit, R. Lan, J. T. S. Irvine and S. Tao, *Adv. Energy Mater.*, **1**(3), 314 (2011).
2. A. Hauch, K. Brodersen, M. Chen and M. B. Mogensen, *Solid State Ionics*, **293**, 27 (2016).
3. M. Guillodo, P. Vernoux and J. Fouletier, *Solid State Ionics*, **127**(1-2), 99 (2000).
4. J. T. S. Irvine, D. Neagu, M. C. Verbraeken, C. Chatzichristodoulou, C. Graves and M. B. Mogensen, *Nat. Energy*, **1**(1), 1 (2016).
5. A. A. E. Hassan, N. H. Menzler, G. Blass, M. E. Ali, H. P. Buchkremer and D. Stöver, *Adv. Eng. Mater.*, **4**(3), 125 (2002).
6. T. Yamaguchi, H. Sumi, K. Hamamoto, T. Suzuki, Y. Fujishiro, J. D. Carter and S. A. Barnett, *Int. J. Hydrogen Energy*, **39**(34), 19731 (2014).
7. N. Ai, Z. Lü, J. Tang, K. Chen, X. Huang and W. Su, *J. Power Sources*, **185**(1), 153 (2008).
8. Y. M. Park, H. J. Lee, H. Y. Bae, J. S. Ahn and H. Kim, *Int. J. Hydrogen Energy*, **37**(5), 4394 (2012).
9. J. Kong, K. Sun, D. Zhou, N. Zhang, J. Mu and J. Qiao, *J. Power Sources*, **166**(2), 337 (2007).
10. E. D. Wachsman and K. T. Lee, *Science*, **334**(6058), 935 (2011).
11. A. V. Virkar, J. Chen, C. W. Tanner and J. W. Kim, *Solid State Ionics*, **131**(1), 189 (2000).
12. S. Molin, A. Chrzan, J. Karczewski, D. Szymczewska and P. Jasinski, *Electrochim. Acta*, **204**, 136 (2016).
13. D. Neagu, T. S. Oh, D. N. Miller, H. Menard, S. M. Bukhari, S. R. Gamble, R. J. Gorte, J. M. Vohs and J. T. S. Irvine, *Nat. Commun.*, **6**, 1 (2015).
14. D. Neagu, G. Tsekouras, D. N. Miller, H. Ménard and J. T. S. Irvine, *Nat. Chem.*, **5**(11), 916 (2013).
15. J. Tan, D. Lee, J. Ahn, B. Kim, J. Kim and J. Moon, *J. Mater. Chem. A*, **6**(37), 18133 (2018).
16. H. Lv, L. Lin, X. Zhang, Y. Song, H. Matsumoto and C. Zeng, *Adv. Mater.*, **1906193**, 1 (2019).
17. J. H. Myung, D. Neagu, D. N. Miller and J. T. S. Irvine, *Nature*, **537**(7621), 528 (2016).
18. L. Lu, C. Ni, M. Cassidy and J. T. S. Irvine, *J. Mater. Chem. A*, **4**(30), 11708 (2016).
19. J. Kim, D. Shin, J. W. Son, J. H. Lee, B. K. Kim, H. J. Je, H. W. Lee and K. J. Yoon, *J. Power Sources*, **241**, 440 (2013).
20. B. A. Rosen, *Electrochem*, **1**(1), 32 (2020).
21. S. Tao and J. T. S. Irvine, *Chem. Rec.*, **4**(2), 83 (2004).
22. R. M. C. Clemmer and S. F. Corbin, *Solid State Ionics*, **166**(3-4), 251 (2004).
23. J. Divisek, R. Wilkenhöner and Y. Volfkovich, *J. Appl. Electrochem.*, **29**(2), 153 (1999).
24. P. Holtappels, C. Sorof, M. C. Verbraeken, S. Rambert and U. Vogt, *Fuel Cells*, **6**(2), 113 (2006).
25. I. Kagomiya, S. Kaneko, Y. Yagi, K. Kakimoto, K. Park and K. H. Cho, *Ionics*, **23**(2), 427 (2017).
26. R. Barfod, M. Mogensen, T. Klemensø, A. Hagen, Y. L. Liu and P.V. Hendriksen, *Proc. - Electrochem. Soc.*, **154**(4), B371 (2007).
27. T. Jia, Z. Zeng, X. Zhang, X. Zhang, P. Ohodnicki, B. Chorpening, G. Hackett, J. Lekse and Y. Duan, *Phys. Chem. Chem. Phys.*, **21**(36), 20454 (2019).
28. M. Bradha, S. Hussain, S. Chakravarty, G. Amarendra and A. Ashok, *J. Alloys Compd.*, **626**, 245 (2015).
29. M. Bradha, S. Hussain, S. Chakravarty, G. Amarendra and A. Ashok, *Ionics*, **20**(9), 1343 (2014).